Influence of Temperature Distribution on Radial Growth of Compressor Discs

Dario Luberti, Hui Tang, James A Scobie, Oliver J Pountney, J. Michael Owen and Gary D. Lock
d.luberti@bath.ac.uk, h.tang2@bath.ac.uk, j.a.scobie@bath.ac.uk, o.j.pountney@bath.ac.uk, ensjmo@bath.ac.uk and g.d.lock@bath.ac.uk
Department of Mechanical Engineering
University of Bath
Bath, BA2 7AY
United Kingdom

ABSTRACT

For the next generation of aero-engines, manufacturers are planning to increase the overall compressor pressure ratio from existing values around 50:1 to values of 70:1. The requirement to control the tight clearances between the blade tips and the casing over all engine-operating conditions is a challenge for the engine designer attempting to minimise tip-clearances losses. Accurate prediction of the tip clearance requires an accurate prediction of the radial growth of the compressor rotor, which depends on the temperature distribution of the disc. The flow in the rotating cavities between adjacent discs is buoyancy-driven, which creates a conjugate heat transfer problem: the disc temperature depends on the radial distribution of Nusselt number, which in turn depends on the radial distribution of disc temperature.

This paper focuses on calculating the radial growth of a simplified compressor disc in isolation from the other components. Calculations were performed using steady one-dimensional (1D) theoretical and two-dimensional finite-element computations (2D FEA) for overall pressure ratios (OPR) of 50:1, 60:1 and 70:1. At each pressure ratio, calculations were conducted for five different temperature distributions; the distribution based on an experimentally-validated buoyancy model was used as the datum case, and results from this were compared with those from linear, quadratic, cubic and quartic power laws.

The results show that the assumed distribution of disc temperature has a significant effect on the calculated disc growth, whereas the pressure ratio has only a relatively small effect. The good agreement between the growth calculated by the 1D theoretical model and the FEA suggests that the 1D model should be useful for design purposes. Although the results were obtained for steady-state conditions, a method is outlined for calculating the growth under transient conditions.

1 INTRODUCTION

Figure 1 is a schematic of a generic HP (high-pressure) compressor rotor in an aero engine [1]. In the external annulus, the compressed air heats the blades and shrouds at the periphery of the discs. At the bore of the discs an axial throughflow of air, extracted from an upstream stage, is used for cooling purposes.

For the next generation of aero-engines, manufacturers are planning to increase the overall compressor pressure ratio from existing values around 50:1 to values of 70:1; this will result in shorter blades. Blade-tip leakage represents a significant source of loss for a turbomachinery stage [2], especially if the rotor is unshrouded, as in aero engine compressor. As the blade height is reduced at the higher pressure ratios, the requirement to control tight clearances between the blade tips and the casing over a wide range of engine-operating conditions is a challenge for the engine designer.

The tip gap $\boldsymbol{G}$ at any operating point is given by a cold-built clearance (when the engine is at an ambient condition) $\boldsymbol{G_{CB}}$, plus the casing radial growth $\boldsymbol{\delta_{CS}}$ (computed at the inner radius), minus the radial growth of the blade tip $\boldsymbol{\delta_{BT}}$:

$$G = G_{CB} + \delta_{CS} - \delta_{BT} \qquad (1)$$

The radial growth of the blade tip δ_{BT} depends strongly on the radial growth of the discs to which the blades are attached. The overall radial growth of a compressor disc,

considered without the blades, depends on the following: (i) the *thermal expansion* δ_E of the material; (ii) the *rotational growth* δ_R due to the stresses created by the rotational speed of the disc; and (iii) the *thermal growth* δ_T of the disc due to the stresses created by the temperature gradients. The *total radial growth* δ_{TOT} of a compressor disc is the sum:

$$\delta_{TOT} = \delta_E + \delta_R + \delta_T \qquad (2)$$

It is the calculation of the thermal growth δ_T - which depends on an estimate of the radial distribution of temperature - that creates the largest uncertainty for the designer.

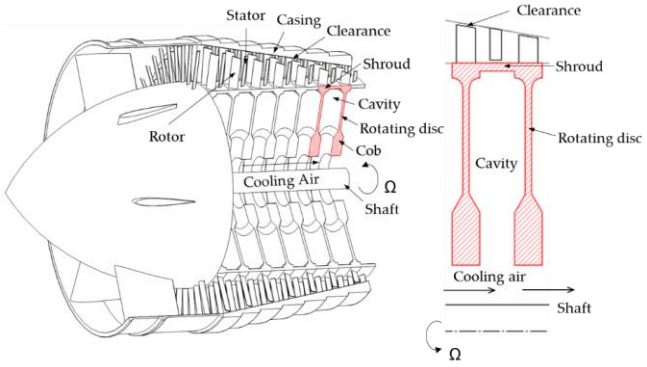

Figure 1: Simplified representation of a high pressure compressor [1]

The object of this paper is to calculate, for different pressure ratios, the effect of temperature distribution on the radial growth of a compressor disc. The temperature distribution based on an experimentally-validated buoyancy model was used as the datum case, and results from this were compared with those from linear, quadratic, cubic and quartic power laws. The growth was determined using 2D FEA (finite-element analysis) and a 1D theoretical stress model.

A literature review is given in Section 2. The disc geometry, model and material are presented in Section 3. The three components of the disc radial growth are computed for a 50:1 pressure ratio, using FEA and the theoretical model in Section 4. In Section

5, the effects of the temperature distributions on the disc growth are calculated for future compressor designs operating at steady conditions for pressure ratios of 60:1 and 70:1. The main conclusions are summarised in Section 6. Appendices A and B summarise the equations used in the buoyancy model and the 1D stress model. Appendix C shows how the method could be extended to predict radial growth under transient conditions.

The definition of symbols not defined in the text below can be found in the Nomenclature.

2 LITERATURE REVIEW

Various simple models have been used to compute the time-response of the tip clearance of the compressor blades during typical aero-engine transients. These simple models are quick to solve, but their accuracy is questionable.

The transient response - during operations such as acceleration from idle to maximum take-off, deceleration and hot re-slam - was considered by Atkins [3]. Agarwal *et al*. [4] used a unique bulk temperature for the whole disc and blades when computing with FEA the tip clearance of a turbine rotor during transient.

Kypuros and Melcher [5] considered an air-cooled turbine disc from idle to maximum power. They assumed that only the external shroud was in contact with the hot annulus gas, and the blades were treated separately to the disc. The radial temperature gradient was neglected - the disc reference temperature was determined by the compressor discharge temperature – and consequently only the disc thermal expansion and the rotational growth were calculated from this model.

Pilidis and Maccallum [6] developed a transient model for both compressors and turbines. They used a correlation to estimate the radial temperature distribution on the

disc, which was simplified into three parts: hub, diaphragm and shroud. The model was not validated against FEA nor experimental data.

Yepifanov *et al.* [7] used a transient model of a complete engine to calculate changes to the turbine performance using empirical correlations for the heat transfer at the disc surfaces. They solved three different 2D models: a full turbine-rotor model, with blades simulated by a distributed force; a single-blade model; and a casing model. The displacements were computed by means of finite element analysis, and the displacements for the three models were subsequently merged to determine the tip clearance.

Dong *et al.* [8] used a steady model to estimate the tip clearance in a multistage axial compressor, validating their results with experimental data. The model was based on three sub-models for the blade, disc and shroud. The shroud sub-model consisted of a ring-element subject to thermal expansion and to the balance between annulus and cavity pressures. Empirical correlations of the Nusselt numbers were used to calculate the disc temperatures.

Figure 1 shows the disc cavities between compressor rotors where the rotating flow is driven by buoyancy effects. Calculation of the disc temperature is a conjugate problem: the heat transfer from the disc is coupled with the air temperature inside the cavity. The buoyancy-induced flow is three-dimensional, unsteady and unstable. Obtaining reliable solutions from computational fluid dynamics is a challenge at the high Grashof numbers, Gr_f, found in modern compressors. Engine designers often rely on empirical equations for the Nusselt number, often based on inappropriate physical models. Recently physically-based theoretical modelling of the buoyancy-induced flow has been used to predict the Nusselt numbers and disc-temperature distributions inside compressor rotors [9-13]. Predictions from these buoyancy models, all of which are for

laminar flow, have been validated using steady flow measurements made in open and closed compressor rigs up to $Gr_f \sim 10^{12}$. Figure 2, taken from [11], compares the predicted nondimensional disc temperatures and Nusselt numbers with experimentally-determined values.

The fact that laminar buoyancy models can be used for large Grashof numbers, where most engineers expect the flow to be turbulent, was attributed to the large Coriolis accelerations in the fluid core and to the fact that there is only a small difference between the rotational speed of the core and that of the discs. As many as 223 separate tests were analysed in the validation of the models, and good agreement between the predictions and measurements was achieved for most cases. In this paper. the buoyancy model is used for cases where $Gr_f > 10^{13}$, beyond the point it has been validated against experiment.

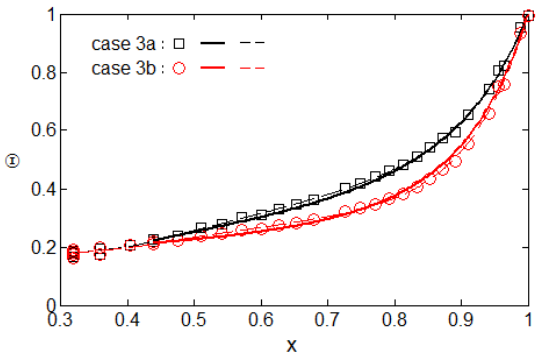

a) Nondimensional temperature

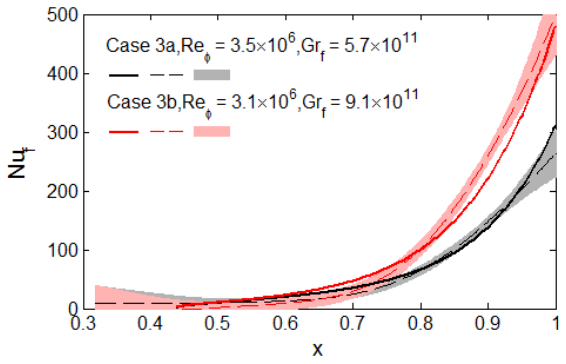

b) Nusselt numbers

Figure 2: Distributions of nondimensional temperature and Nusselt numbers for $Ro \approx 0.6$. (Symbols denote measured temperatures; broken and solid lines represent experimental and theoretical results respectively; shading shows 95% confidence intervals on experimental Nusselt numbers) [11].

3 DISC MODELING AND METHODOLOGY

Here the modelling and methodology to determine the disc stresses and growth are presented. The disc geometry is taken from that published by the University of Sussex.

3.1 Geometry and material

The multi-cavity rig at the University of Sussex, which was made from titanium, is a 70% model-to-engine scale of a compressor cavity stack similar to that found in a Trent engine, as reported by Alexiou [14], Long *et al.* [15], and Atkins and Kanjirakkad [16]. The dimensions for the disc considered here were for the 100% engine size.

The disc comprised three parts: a thick hub, a thin diaphragm and a peripheral shroud; fillets were used to blend the geometry at the two interfaces. The shroud radial thickness was assumed equal to that of the diaphragm and a summary of the dimensions of the disc is given in Figure 3.

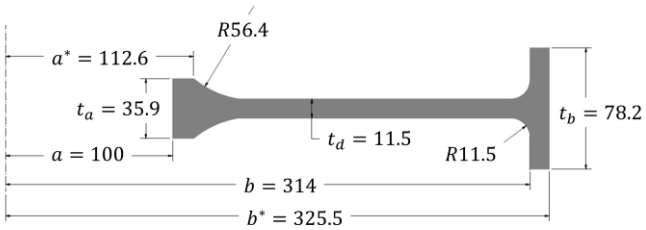

Figure 3: Dimensions of the disc model (mm)

Cumpsty [17] reported that titanium alloys are not suitable for the last two HP compressor discs of modern aero-engines where the temperatures are higher than 870 K. Inconel 718, which is one of the super-alloys widely used in turbomachinery rotors [18], is the material used for the discs considered here. The physical properties of Inconel 718 as a function of temperature are shown in Table 1. The variation of density in the analysed temperature range is low compared to the other physical properties and is therefore neglected.

	21°C	93°C	204°C	316°C	538°C	649°C
ρ [kg/m^2]				8193		
E [GPa]	204	199	194	187	176	169
υ	0.294	0.288	0.280	0.272	0.271	0.283
α [10^{-5} °C^{-1}] (from ambient)	/	1.28	1.35	1.39	1.44	1.51
k [W/(m°C)]	11.0	12.4	14.2	16.0	19.5	21.2

Table 1: Properties of Inconel 718

The results presented here were obtained assuming constant properties independent of temperature. The values in the table were linearly interpolated and calculated at the mean temperature between the disc bore and the outer shroud. Extended FEA computations, not shown here, revealed that the constant-property results were not significantly different from those that were temperature dependent.

The FEA was conducted using Ansys v18.1 for a 2D axisymmetric disc. Using centreline symmetry, only half the disc geometry shown in Figure 3 was modelled. The chosen element size was 0.4 mm, resulting in ~ 12,000 elements. Grid independence was verified by the repeatability of the temperature, stresses and growth calculations with smaller element sizes.

For the buoyancy model and the 1D stress model, the fillets shown in Figure 3 were removed. The disc was reduced to three rectangular parts: a thick hub, a thin diaphragm, and a shroud.

3.2 Application of buoyancy model

The principal equations used in the buoyancy model are given in Appendix A. The model was used, together with a 1D circular fin equation, to predict the radial temperature distribution and the Nusselt numbers of the compressor disc.

The model requires a cavity air pressure at $r = a$, and disc temperatures at $r = b$ and $r = a$ (see Figure 3). The assumptions made to produce these values are given below for a flight Mach number of 0.85 and a cruise altitude of 10,000 m, with an ambient static air temperature and pressure of -50 ˚C and 0.265 bar respectively. The rotational speed of the compressor was taken to be 10,000 rpm.

The cavity static air pressure at $r = a$ was assumed equal to that of the axial throughflow of cooling air at the centre of the cavity (see Figure 1). This was taken to be the pressure after the IPC (intermediate pressure compressor); for an OPR = 50 this is typically about 14 times the engine inlet total pressure. The cavity air pressure was assumed to increase proportionally with OPR. The air temperature for the final stages of the HPC and IPC were calculated from the pressure ratio and a polytropic efficiency of 0.95.

The ratio of the temperature differences between the disc bore and the HPC, and between the IPC and the HPC, were assumed to be constant at 0.3 for all OPRs. This leads to a constant value of $\beta\Delta T$ ~ 0.3, which is a typical value for HPCs [13]. The disc temperature at $r = b$ was assumed to be the same as the temperature of the inner surface of the shroud; this inner temperature was estimated using 1D heat transfer through the shroud. The model requires a Coriolis parameter, *Co*, and a value of 0.030 was chosen to match engine-representative conditions [13].

A cautionary note is added here. The above assumptions are used to produce values that are thought to be representative of those in aeroengine compressors; the actual values are unknown. In addition, it should be noted that the Grashof numbers based on the above assumed values are around 1.5 x 10^{13}, whereas the buoyancy model has only been validated for values up to 10^{12}.

3.3 FEA calculation of temperature distribution

The heat transfer coefficients used here were derived from the Nusselt numbers calculated from the buoyancy model. The boundary conditions are indicated in Figure 4.

- A: Radial distribution of heat transfer coefficient from the inner radius to the inner shroud radius, including the fillet.
- B: Adiabatic centreline for symmetry.
- C: Adiabatic boundary at edge of the shroud.
- D: Inner shroud heat transfer coefficient.
- E: HPC temperature at the outer shroud, to simulate the thermal effect of the hot annulus flow.
- F: $T = T_a$ at the disc bore.

The buoyancy model, together with the 1D fin equation, gives both the disc temperature and the Nusselt numbers, from which the heat transfer coefficients, h_f, were calculated. Figure 5 shows that the temperatures obtained from the buoyancy model are in good agreement with those produced from the FEA, using the above values of h_f. Note that the fillets alter the disc area exposed to the heat transfer.

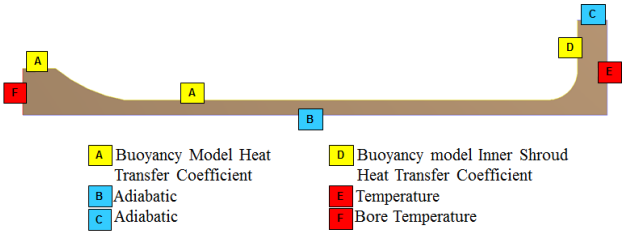

Figure 4: Thermal FEA model and boundary conditions

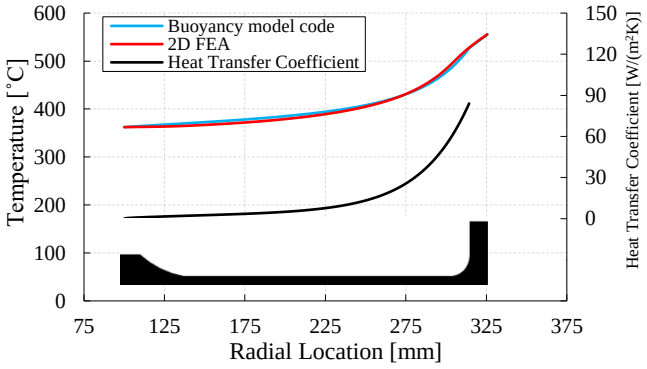

Figure 5: Variation of disc temperature with radius: comparison of FEA and buoyancy model for OPR = 50. Temperature from the FEA taken at the centreline

3.4 1D stress model

The geometry used in the 1D stress model was the same as that shown in Figure 3 but without fillets. The stresses and radial growth of the discs were calculated at 10,000 rpm using the temperature distribution predicted by the buoyancy model.

The disc was divided into three subparts: hub, diaphragm and shroud. The radial stress σ_r, the tangential stress σ_t and the total radial growth δ_{TOT} can be expressed as functions of the disc radius for each subpart (see Appendix B). These functions are the general stresses and growth equations for a constant-thickness rotating disc with a temperature distribution [19]. They were determined with known integration constants. There are two constants for each subpart, resulting in a linear system of six equations with six unknowns. The boundary conditions are as follows:

- As no blades are considered, the radial stress for the shroud at $r = b^*$ is equal to zero
- As the disc is not constrained at $r = a$, the radial stress for the hub at $r = a$ must be zero
- For the radial equilibrium at the shroud – diaphragm interface, the radial stress at the shroud is equal to the radial stress at the diaphragm, with t_d/t_b the scaling factor. There is a similar scenario at the hub – diaphragm interface, with t_d/t_a the scaling factor. These result in two boundary conditions.
- The geometric compatibility implies that the radial growth at $r = b$ (see Figure 3) for the shroud and for the diaphragm must be the same; there is a similar scenario at $r = a^*$. This results in two further boundary conditions.

The calculated radial and circumferential stresses (denoted by σ_r and σ_t), and radial growth δ_{TOT}, are shown in Section 4 as functions of the radius.

Solving the problem for a constant disc temperature isolates the stresses and growth due to rotation; these are denoted by $\sigma_{r,R}$, $\sigma_{t,R}$ and δ_R. For the case of constant

temperature and no rotation, the growth is reduced to the thermal expansion of the disc from a reference temperature (the cold-built temperature, $T_{CB} = 15\ ^{\circ}C$). The disc inner temperature T_a (again with no rotation) is taken as the reference temperature, and the solution of the system represents the thermal expansion δ_E, with the associated stresses $\sigma_{r,E}$ and $\sigma_{t,E}$ equal to zero.

Finally, consider the case of imposing only the temperature distribution from the buoyancy model; the thermal stresses $\sigma_{r,T}$ and $\sigma_{t,T}$ are retrieved, but the resulting thermal growth will be the sum $\delta_E + \delta_T$, from which the thermal growth δ_T is computed.

The thermal stresses and growth depend only on the radial temperature gradients and not on the actual temperature extremes. That is, the thermal growth depends only on the *shape* of the radial temperature profile.

Referring to equation (1), it follows that:

$$\sigma_r = \sigma_{r,R} + \sigma_{r,T} \qquad (3)$$

$$\sigma_t = \sigma_{t,R} + \sigma_{t,T} \qquad (4)$$

3.5 FEA stress and growth calculation

The geometry used in the 2D FEA model was the same as that shown in Figure 3. The stresses and radial growth of the discs were calculated at 10,000 rpm using the temperature distribution predicted by the buoyancy model. There was no axial displacement on the centreline.

4 COMPARISON BETWEEN FEA AND 1D MODEL FOR OPR = 50:1

The results for the FEA are compared with those for the 1D model at cruise conditions and an OPR 50:1. This OPR is typical of state-of-art turbofan engines.

Figure 6 shows the variation of the radial and tangential stress with disc radius, comparing the solutions from the 1D theoretical model and the 2D FEA. There is general qualitative and quantitative agreement between the two solutions. The largest differences occur at the hub – diaphragm interface and at the diaphragm – shroud interface where the 1D theoretical model does not account for the fillet radii. The fillets remove the non-physical discontinuities in stress and reduce the tangential stress at all radii of the disc.

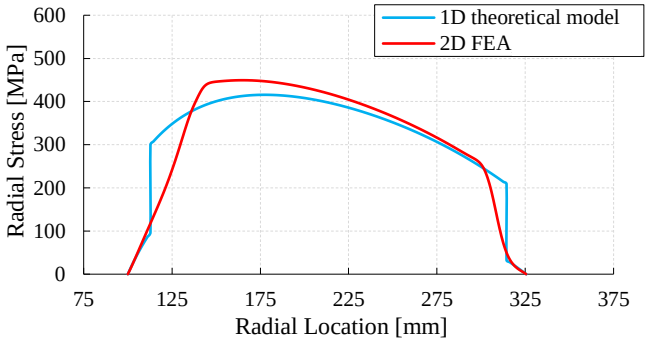

a) Radial stresses

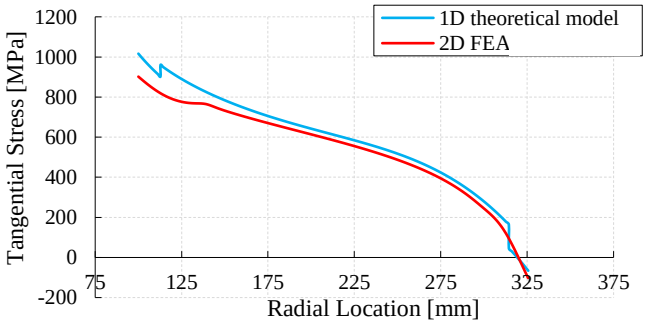

b) Tangential stresses

Figure 6: Comparison of radial and tangential stresses from the 1D theoretical model and 2D FEA (OPR = 50)

Calculations were performed to isolate the rotational and thermal stresses; these are shown in Figures 7 and 8 respectively. Qualitatively, there are similar features to those discussed above for Figure 6. The stress equations, Eqs (3 & 4) have a linear solution;

thus the sum of both the radial and tangential stresses in Figures 7 and 8 are equal to the radial and tangential stresses in Figure 6.

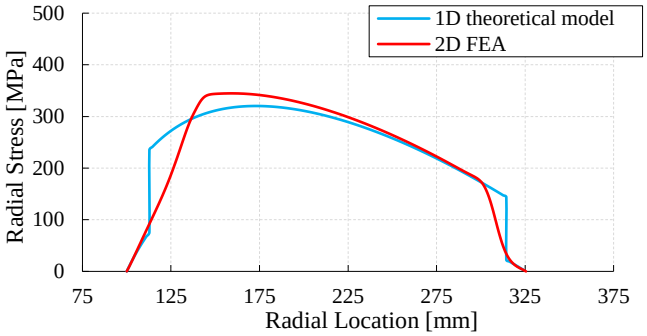

a) Rotational part of the radial stresses

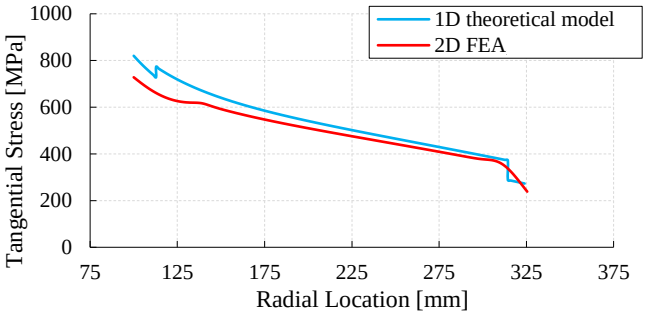

b) Rotational part of the tangential stresses

Figure 7: Comparison of rotational stresses from 1D theoretical model and 2D FEA (OPR = 50)

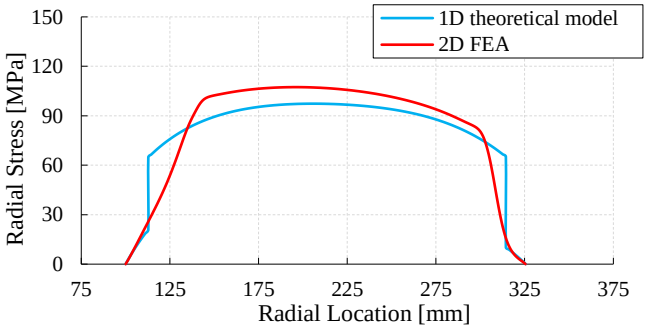

a) Thermal part of the radial stresses

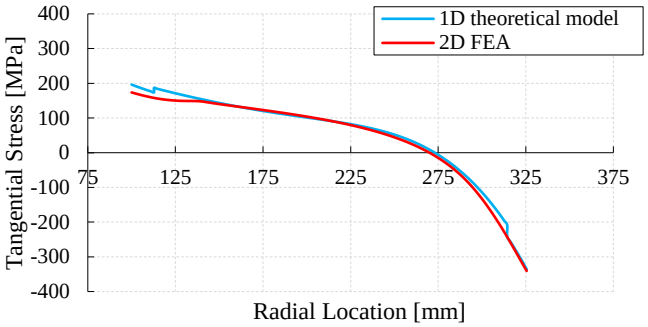

b) Thermal part of the tangential stresses

Figure 8: Comparison of thermal stresses from 1D theoretical model and 2D FEA (OPR = 50)

The total radial growth of the disc with all components expressed in Eq. (2) is shown in Figure 9. The total growth is the sum of the rotational growth, the thermal growth and the thermal expansion. For a given temperature difference, the thermal expansion only depends linearly on the radius; hence the corresponding curves for this element collapse for all the three cases. The 1D theoretical model slightly overestimates the other growth components relative to the 2D FEA.

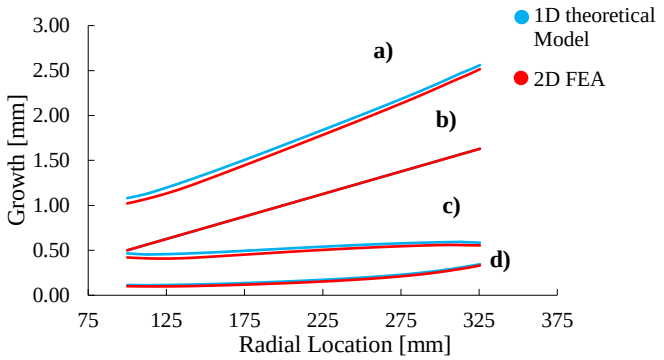

Figure 9: Variation of disc growth as a function of radius: a) total; b) thermal expansion; c) rotational growth; d) thermal growth. (OPR = 50)

A summary of the growths at the outer radius is shown in Table 2. The thermal expansion is the largest component, followed by the rotational and the thermal growth. The average difference between the 1D and FEA growths is around 6%.

	Thermal Expansion [mm]	Rotational Growth [mm]	Thermal Growth [mm]	Total Growth [mm]
Theoretical Model	1.58	0.58	0.35	2.51
FEA	1.58	0.55	0.33	2.46

Table 2: Growth components at disc outer radius

(OPR = 50)

The tip clearance of a compressor blade can be expressed relative to the blade chord or the blade height. These ratios change over the full range of engine operating conditions. For the last compressor stage of a large turbofan engine, these values are around 1% of the chord before, and 3% after, the endurance test [20]. With measurement-based predictions, the same reference reports, again for the last compressor stages, a tip clearance of 0.4 and 0.1 mm for respectively 90% and 95% of the nominal rotational speed. According to Dong *et al*. [7], the last (tenth) rotor of an HP compressor has a measured running clearance of 0.3 mm. The thermal growth in Table 2 is of the same scale as the running tip clearances reported for engines. Importantly, this growth is directly related to the assumed temperature distribution over the compressor disc.

The combined solution of the coupled 1D stress and buoyancy equations took only seconds to solve on a laptop. The good agreement between the growths predicted by the 1D theoretical model and the FEA computations suggests that the combination of the 1D model and the buoyancy model should be useful in the preliminary calculation of blade clearances. However, as shown below, the accuracy of the predicted thermal growth depends on the accuracy of the predicted temperature distribution.

5 EFFECT OF OPR AND TEMPERATURE DISTRIBUTION

In the previous section, the temperature distribution based on an experimentally-validated buoyancy model was used. In this section, all results were obtained using FEA.

The results from the datum case are compared below with those obtained using power-law temperature profiles. Power laws, which are often used for simplicity for the temperature distributions of rotating discs, provide a reasonable approximation to the temperature predictions obtained from the validated buoyancy model. However, although power laws might be suitable for the steady-state cases considered here, no single power law could fit the changing temperature profile during a thermal transient.

Since higher pressure ratios increase the temperatures and Nusselt numbers, predictions were extended up to OPR = 70. The Grashof numbers for each pressure ratio (50:1, 60:1 and 70:1) were 1.2×10^{13}, 1.5×10^{13} and 1.7×10^{13}.

The generic power-law profile is given by

$$T(r) = T_a + K(r - a)^n \qquad (5)$$

Here the constant K for each value of n is determined by imposing the relevant outer-shroud temperature, which is assumed to be the total temperature in the HPC. The exponent n determines the *shape* of the profile, which determines the thermal stress. The power laws considered are linear, quadratic, cubic and quartic (*i.e.* $n = 1,2,3,4$

Neither the change of temperature profile nor the overall pressure ratio alters the rotational growth, δ_R, which depends only on rotational speed (assumed constant here). However, the thermal expansion δ_E, is affected by the OPR, as the temperature at the bore (T_a) increases with OPR. The thermal growth δ_T is affected by both the temperature distribution and the OPR.

Figures 10-12 show the variation of thermal growth with radial position for OPR = 50, 60 and 70, respectively. These figures illustrate the effect of the different temperature profiles. In all cases the buoyancy model, which is used as a datum, yields a thermal growth bounded by those obtained from the temperature profiles for n = 3 and 4. Generally, results from the buoyancy model are very close to the n = 3 power law at the lower radii, with some deviation at the higher radii. At higher OPR (towards 70:1) results from the buoyancy model are very close to the n = 4 power law.

Figure 13 shows the variation of calculated thermal growth at the disc outer radius with OPR. The gradient of the thermal growth obtained using the buoyancy model is lower than any analysed power law. The model thus gives a thermal growth which is less sensitive to the overall pressure ratio.

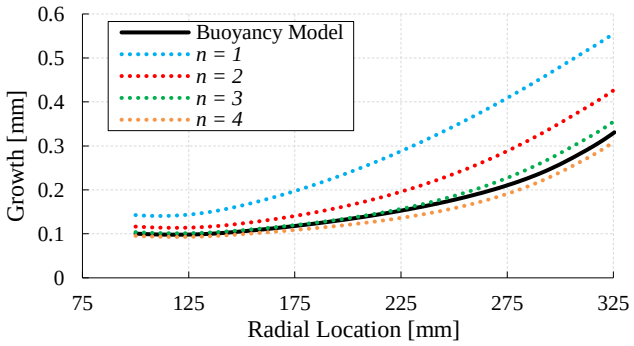

Figure 10: OPR = 50: Comparison between thermal growths determined from buoyancy model and power law temperature profiles

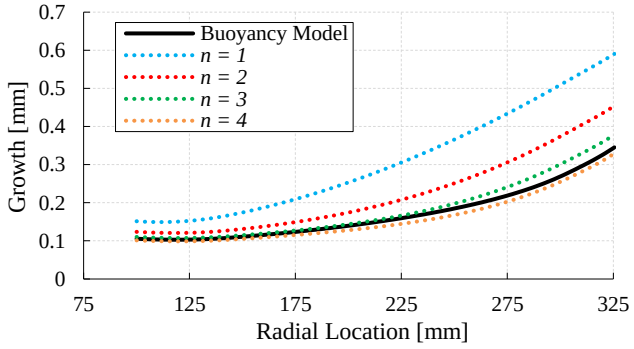

Figure 11: OPR = 60: Comparison between thermal growths determined from buoyancy model and power law temperature profiles

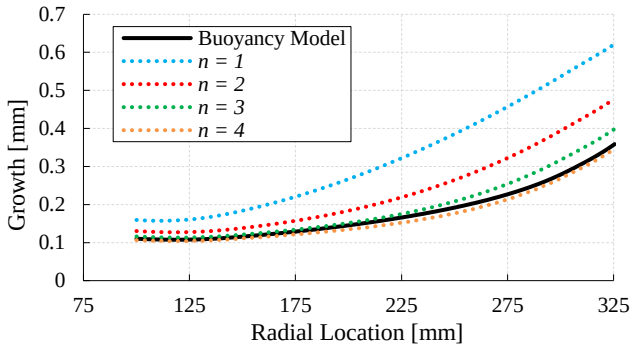

Figure 12: OPR = 70: Comparison between thermal growths determined from buoyancy model and power law temperature profiles

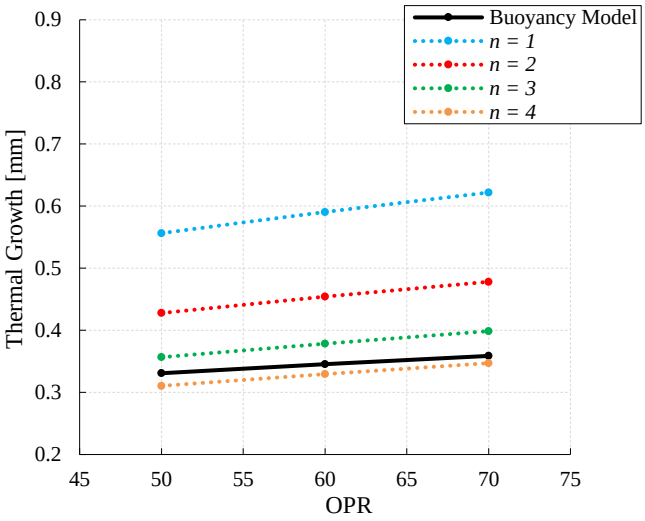

Figure 13: Variation of thermal growth at disc outer radius with OPR

Table 3 shows the thermal expansion, thermal growth, and the total growth calculated at the outer-shroud radius from the different temperature profiles at the three OPRs. The total growth includes the rotational growth. At OPR = 50, the buoyancy model yields a thermal growth bounded by those obtained from the temperature profiles for n = 3 and 4; at 70:1 the calculations are much closer to that determined from the n

= 4 order profile. By contrast, a linear power-law causes errors the same magnitude as the thermal growth itself.

	OPR = 50		OPR = 60		OPR = 70	
Thermal Expansion	1.58		1.76		1.92	
	Thermal	Total	Thermal	Total	Thermal	Total
Buoyancy Model	0.33	2.47	0.34	2.66	0.36	2.85
$n = 1$	0.56	2.70	0.59	2.91	0.62	3.11
$n = 2$	0.43	2.57	0.45	2.77	0.48	2.97
$n = 3$	0.36	2.50	0.38	2.70	0.40	2.89
$n = 4$	0.31	2.45	0.33	2.65	0.35	2.84

Table 3: Effect of temperature distribution and pressure ratio on thermal expansion, thermal growth and total growth of the disc; values in mm

6 CONCLUSIONS

The blade clearances in a compressor depend strongly on the radial growth of the discs to which the blades are attached. The overall radial growth of a compressor disc depends on: (i) the *thermal expansion* of the material; (ii) the *rotational growth* due to the stresses created by the rotational speed of the disc; and (iii) the *thermal growth* of the disc due to the stresses created by the temperature gradients. For (iii), the temperature gradients depend on the Nusselt numbers created by the buoyancy-induced rotating flow in the fluid core in the cavity between adjacent discs. As the Nusselt numbers depend on the radial temperature distribution in the disc, this is a complex conjugate problem, which represents a challenge for the designer.

In this paper, the three growth components were calculated separately for a single disc operating at the steady-state conditions associated with compressor pressure ratios of 50, 60 and 70 to 1. At each pressure ratio, calculations were conducted for five different temperature distributions: the distribution based on a published physically-based buoyancy model was used as the datum case, and results from this were compared with those from linear, quadratic, and cubic and quartic power laws. For the 50:1 pressure ratio, the calculations were conducted using both FEA and a theoretical 1D stress model.

- For the cases considered here, the main conclusion is that the radial distribution of temperature has a significant effect on the disc growth and consequently on the blade clearance in a compressor. Although the growth due to the thermal stress is small relative to the total growth of the disc, it is the same magnitude as the blade clearance.
- Using the buoyancy model as a datum for comparison with the growth predicted using power-law temperature distributions shows that a quartic power-law produces the most accurate results. By contrast, a linear power-law causes errors the same magnitude as the thermal growth itself. (Although a power-law profile might be suitable for the steady-state cases considered here, no single power law could fit the changing temperature profile during a thermal transient.)
- For the assumptions used in the calculations, the pressure ratio has a relatively small effect on the thermal growth.
- There was good agreement between the growths predicted by the 1D theoretical model and the FEA computations. This suggests that the combination of the 1D model and the buoyancy model could be useful in the preliminary calculation

of blade clearances. (The combined solution of the coupled 1D stress and buoyancy equations took only seconds to solve on a laptop.)

Caveat: the results presented in this paper were based on conditions thought to be representative of those in aeroengine compressors; they might not apply to actual conditions. In addition, it should be noted that the Grashof numbers based on the assumed conditions were higher than the values used to validate the buoyancy model.

The authors are currently commissioning a compressor rig at the University of Bath. As well as other measurements, the radial growth of the discs will be determined under steady-state and transient conditions. (An outline of a method that could be used to calculate the disc growth under transient conditions is included in Appendix C.)

FUNDING SOURCE

The authors would like to thank the Engineering and Physical Science Research Council (EPSRC) for their financial support (Project Code No. EP/P003702/1).

Due to confidentiality agreements with research collaborators, supporting data can only be made available to bona fide researchers subject to a nondisclosure agreement. Details of how to request access are available at the University of Bath data archive: http://dx.doi.org/10.15125/BATH-00116.

NOMENCLATURE

a	disc inner radius
A	Area
a^*	diaphragm inner radius
b	diaphragm outer radius

b^* disc outer radius

c specific heat capacity

C_1,C_2 constants for the 1D stress model

Co Coriolis parameter

E Young's modulus

G gap between the blade tip and casing

Gr_c Grashof number in theory

$$(= \frac{\rho_{c,b}^2 \Omega_c^2 b^4}{\mu_{c,b}^2} \frac{T_o - T_{c,b}}{T_{c,b}})$$

Gr_f Grashof number in experiments

$$(= \left(1 - \frac{a}{b}\right)^3 Re_\phi^2 \beta \Delta T)$$

h_c heat transfer coefficient $(= q_o/(T_o - T_c))$

h_f heat transfer coefficient $(= q_o/(T_o - T_f))$

$\bar{h}$ area-averaged heat transfer coefficient

I integral in the buoyancy model

K temperature distribution constant

k thermal conductivity of air

k_s thermal conductivity of disc

Ma_c Mach number in core $(= \Omega_c b/\sqrt{\gamma R T_{c,b}})$

n power-law exponent

Nu_c Nusselt number in theory $(= h_c r/k)$

Nu_f Nusselt number in experiments $(= h_f r/k)$

r radius

R gas constant for air

Re_ϕ rotational Reynolds number $(= \rho_f \Omega b^2/\mu_f)$

Ro	Rossby number ($=\frac{W}{\Omega}a$)
T	temperature
t	thickness
V	volume
W	axial velocity of throughflow
x	nondimensional radius ($= r/b$)
α	thermal expansion coefficient
βΔT	buoyancy parameter ($= (T_{o,b} - T_f)/T_f$)
γ	ratio of specific heats
δ	radial growth
θ	nondimensional disc temperature in theory ($= (T_o - T_c)/(T_{o,b} - T_{c,b})$)
Θ	nondimensional disc temperature in experiment ($= (T_o - T_f)/(T_{o,b} - T_f)$)
ν	Poisson's ratio
ρ	density
σ	normal stress
τ	time constant
Ω	rotational speed of disc

Subscripts

a	value at $r = a$
b	value at $r = b$
BT	blade tip
c	fluid core

CB cold-built

CS casing

d diaphragm

E expansion

f reference value

o disc surface

r radial

R rotation

SS steady-state

t tangential

T thermal

TOT total

Acronyms

FEA Finite-Element Analysis

HP High Pressure

HPC High Pressure Compressor

IPC Intermediate Pressure Compressor

OPR Overall Pressure Ratio

REFEENCES

[1] Owen, J., M., Tang, H., Lock, G., D., 2018, "Buoyancy-Induced Heat Transfer inside Compressor Rotors: Overview of Theoretical Models", Aerospace, 5, 32.

[2] Denton, J., D., 1993, "Loss Mechanisms in Turbomachinery", ASME, 93-GT-435.

[3] Atkins, N., R., 2013, “Investigation of a Radial-Inflow Bleed as a Potential for Compressor Clearance Control”, Proceedings of ASME Turbo Expo, GT2013-95768, June 3-7, San Antonio, Texas, USA.

[4] Agarwal, H., Akkaram, S., Shetye, S., McCallum, A., 2008, “Reduced Order Clearance Models for Gas Turbine Applications”, 49th AIAA/ASME/ASCE/ AHS/ASC Structures, Structural Dynamics, and Materials Conference, 7 – 10 April 2008, Schaumburg, IL, AIAA 2008-2177.

[5] Kypuros, J., A., Melcher, K., J., 2003, “A Reduced Model for Prediction of Thermal and Rotational Effects on Turbine Tip Clearance”, NASA/TM–2003-212226.

[6] Pilidis, P., Maccallum, N., R., L., 1984, “A Study of the Prediction of Tip and Seal Clearances and their Effects in Gas Turbine Transients”, ASME, 84-GT-245.

[7] Yepifanov, S., V., Zelenskyi, R., L., Loboda, I., 2015, “Modeling the Gas Turbine Engine under Its Dynamic Heating Conditions”, Journal of Engineering for Gas Turbines and Power, Vol. 137, 031506.

[8] Dong, Y., Xinqian, Z., Qiushi, L., 2014, “An 11-stage axial performance simulation considering the change of tip clearance in different operating conditions”, Proceedings IMechE Part A: Journal of Power and Energy, Vol. 228(6) 614-625.

[9] Owen, J., M., Tang, H., 2015, “Theoretical Model of Buoyancy-Induced Flow in Rotating Cavities”, Journal of Turbomachinery, Vol. 137, 11105.

[10] Tang, H., Shardlow, T., Owen, J., M., 2015 “Use of Fin Equations to Calculate Nusselt Numbers for Rotating Disks”, Journal of Turbomachinery, Vol. 137, 121003.

[11] Tang, H., Owen, J., M., 2017, “Effect of Buoyancy-Induced Rotating Flow on Temperatures of Compressor Disks”, Journal of Engineering for Gas Turbines and Power, Vol. 139, 062506.

[12] Tang, H., Owen, J., M., 2018, “Theoretical Model of Buoyancy-Induced Heat Transfer in Closed Compressor Rotors”, Journal of Engineering for Gas Turbines and Power, Vol. 140, 032605.

[13] Tang, H., Puttock-Brown, M., R., Owen, J.M., 2018, “Buoyancy-Induced Flow and Heat Transfer in Compressor Rotors”, Journal of Engineering for Gas Turbines and Power, Vol. 140, 071902.

[14] Alexiou, A., 2000, “Flow and Heat Transfer in Gas Turbine H.P. Compressor Internal Air Systems”, PhD Thesis, University of Sussex.

[15] Long, C., A., Miché, N., D., D., Childs, P., R., N., 2007, “Flow measurements inside a heated multiple rotating cavity with axial throughflow”, International Journal of Heat and Fluid Flow, 28, 1391-1404.

[16] Atkins, N., R., Kanjirakkad, V., 2014, “Flow in a Rotating Cavity with Axial Throughflow at Engine Representative Conditions”, Proceedings of ASME Turbo Expo, GT2014-27174, June 16 – 20, Düsseldorf, Germany.

[17] Cumpsty, N., 2003, “Jet Propulsion. A simple guide to the aerodynamic and thermodynamic design and performance of jet engines”, Cambridge University Press.

[18] Muktinutalapati, N., R., 2011, “Materials for Gas Turbines – An Overview”, Advances in Gas Turbine Technology, 293-314.

[19] Vullo and Vivio, 2013, “Rotors: Stress Analysis and Design”, Springer, 57.

[20] Baghdadi, S., 1996, “Modeling Tip Clearance Effects in Multistage Axial Compressors”, Journal of Turbomachinery, Vol. 118, 697-705.

APPENDIX A: EQUATIONS FOR BUOYANCY MODEL

The model assumes that the buoyancy-induced flow in a rotating cavity is controlled by the Ekman-layer flow in the boundary layers on the discs [9]. It also assumes that the rotating flow in the fluid core outside the Ekman layers is adiabatic.

The Nusselt numbers for heat transfer from the disc to the core is given by:

$$\mathrm{Nu_c} = \frac{1}{2}\frac{x_a^{1/2}}{I^{1/4}}\mathrm{Gr}_c^{1/4}\left[(\theta - \mathrm{Co})\left(\frac{\rho_c}{\rho_{c,b}}\right)^2 x^5\right]^{1/3} \qquad \text{(A1)}$$

where $\mathrm{Gr_c}$, the Grashof number, Co, the Coriolis parameter, θ, a nondimensional temperature, *I*, an integral, and the density ratio are defined below:

$$\mathrm{Gr_c} \stackrel{\text{def}}{=} \frac{\rho_{c,b}^2\Omega_c^2 b^4}{\mu_{c,b}^2}\,\frac{T_o - T_{c,b}}{T_{c,b}} \qquad \text{(A2)}$$

$$\mathrm{Co} \stackrel{\text{def}}{=} 2\left(1 - \frac{\Omega_c}{\Omega}\right)\frac{T_{c,b}}{T_{o,b} - T_{c,b}} \qquad \text{(A3)}$$

$$\theta = \frac{T_o - T_c}{T_{o,b} - T_{c,b}} \qquad \text{(A4)}$$

$$I = \int_{x_a}^{1} x^{11/3}\left[(\theta - Co)\left(\frac{\rho_c}{\rho_{c,b}}\right)^2\right]^{1/3} dx \qquad \text{(A5)}$$

$$\frac{\rho_c}{\rho_{c,b}} = \left[\frac{1 + \frac{\gamma-1}{2}Ma_c^2(x^2 - x_a^2)}{1 + \frac{\gamma-1}{2}Ma_c^2(1 - x_a^2)}\right]^{1/(\gamma-1)} \qquad \text{(A6)}$$

The Coriolis parameter, which can be thought of as the ratio of Coriolis forces to buoyancy forces, is treated as an empirical constant. The integral *I* represents the momentum exchange between the flow in the core and that in the Ekman layers on the discs. Equation (A5) for the density ratio is based on the assumption that the flow in the core is adiabatic.

This is a conjugate problem, and the nondimensional temperature, θ, couples the heat transfer from the disc to the temperature difference between the disc and the core. Knowing $\mathrm{Nu_c}$, the disc temperature can be calculated using the circular fin equation [10]. This involves iteration until there is convergence between Nu_c and θ.

APPENDIX B: EQUATIONS FOR 1D STRESSES AND GROWTH

Considering the effects of the thermal expansion, rotation and temperature gradients, the general equations for the radial stress, tangential stresses and radial growths are [19]:

$$\sigma_r(r) = -\frac{3+v}{8}\, r^2\rho\Omega^2 - \frac{\alpha E}{r^2}\int_a^{b^*}(T-T_{CB})rdr + \frac{C_1 E}{2(1-v)} - \frac{C_2 E}{r^2(1+v)}\sigma_r \tag{B1}$$

$$\sigma_t(r) = -\frac{1+3v}{8}\, r^2\rho\Omega^2 + \alpha E\left[\frac{1}{r^2}\int_a^{b^*}(T-T_{CB})rdr - (T-T_{CB})\right] + \frac{C_1 E}{2(1-v)} + \frac{C_2 E}{r^2(1+v)} \tag{B2}$$

$$\delta(r) = -(1-v^2)\frac{r^3\rho\Omega^2}{8E} + \frac{\alpha(1+v)}{r}\int_a^{b^*}(T-T_{CB})rdr + C_1\frac{r}{2} + \frac{C_2}{r} \tag{B3}$$

These equations, which are valid for a constant-thickness disc, can be specified for the hub, diaphragm and shroud, obtaining three pairs of unknown integration constants (C_1 and C_2 for each subpart). The first term of each of the eqs [B1-B3] accounts for the rotation, the second for the temperature distribution, the last two terms are the

homogeneous term, defined by the boundary conditions. The unknowns are determined using the constraints described in section 4.3. The radial growth of the disc δ_{TOT} is the value of $\delta(r)$ at $r = b^*$.

APPENDIX C: APPLICATION OF THE METHOD FOR TRANSIENT CONDITIONS

Aircraft engines are required to maintain the performance and avoid damages during all transient conditions. The incompatibility in thermal inertia between the HPC rotor and the casing, together with the changing engine speed, can result in minima in the tip clearance, with the possibility of rub. This flight scenario is often referred to "hot re-slam."

A typical transient approach for rotor growth calculation consists in modelling the single rotor parts with concentrated – or "lumped" – parameters [6, 7] - which involves a constant temperature and a single time constant for an entire compressor disc. That approach provides no details of the temperature *gradient*, and hence it cannot calculate the transient thermal growth. The method outlined below can be used together with a lumped transient model to show the transient response of each growth component.

First, the buoyancy model is solved for the initial and final steady-states to calculate the two separate distributions of the radial temperature and heat transfer coefficient. The area-averaged heat transfer coefficients are then used to estimate a time-constant, τ, for each steady-state ([3]):

$$\tau = \frac{\rho V c}{\bar{h} A} \qquad \text{(C1)}$$

The time-constant for the whole transient evolution is assumed to be the mean of the two values. The transient temperature is then given by:

$$T(r, time) = T_{SS1}(r) + [T_{SS2}(r) - T_{SS1}(r)](1 - e^{-\frac{time}{\tau}}) \quad \text{(C1)}$$

This equation can then be applied to a transient finite-element simulation to calculate the transient growth.

A realistic flight scenario is when a reduction of cruise speed occurs, and the initial and final steady-states (SS1 and SS2) are reported in Table C1. The calculated mean time-constant is about 15 minutes, and Figure C1 shows the corresponding steady temperature distributions.

	SS1	SS2
Altitude [m]	10,000	10,000
N [rpm]	10,000	9,500
OPR	50	45
Flight Mach number	0.85	0.77

Table C1 – Cruise steady-states considered for the transient analysis

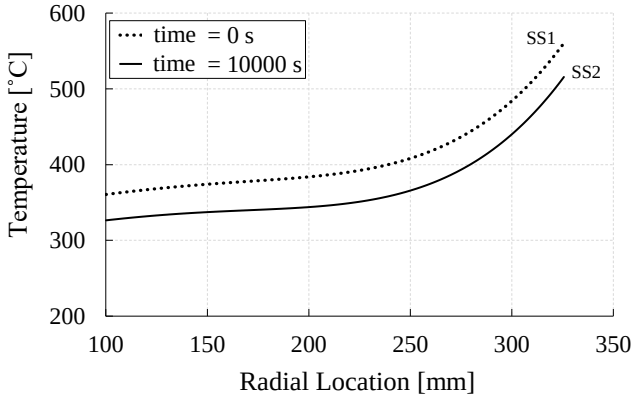

Figure C1 – Initial (SS1) and final (SS2) temperature distributions

In an engine manoeuvre, the rotational growth is the fastest to respond, and a deceleration of 50 rpm/s is assumed. After applying the interpolated transient temperature history from SS1 to SS2 using eq. (C1), the transient radial growths –

calculated using FEA – are shown in Figure C2. The rotational growth decreases with decreasing speed, and the thermal expansion also decreases owing to the monotonic decrease of the bore temperature caused by deceleration. The thermal growth depends on the temperature gradient of the initial and final states, and – as the temperature gradient is lower at SS2 – the thermal growth decreases.

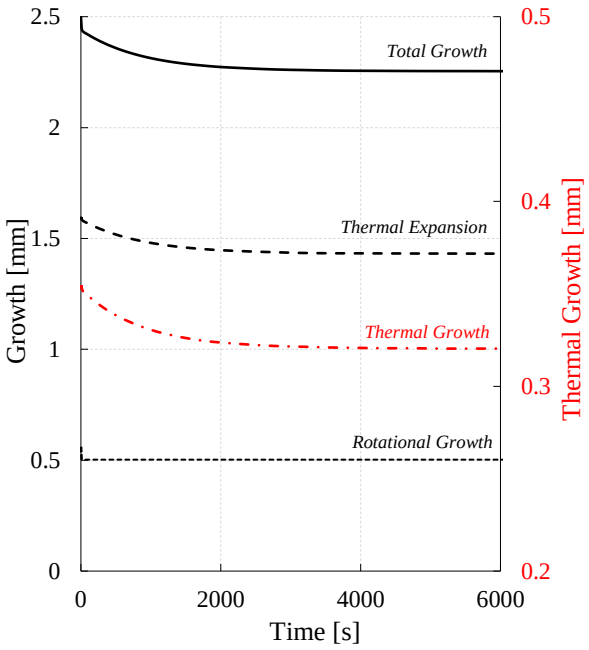

Figure C2 – Transient response of the disc growth components for a cruise speed reduction